Volume 3 | Number 6 | December 2018 | Pages 871–972

Molecular Systems Design & Engineering

Building and designing systems from the molecular level

rsc.li/molecular-engineering

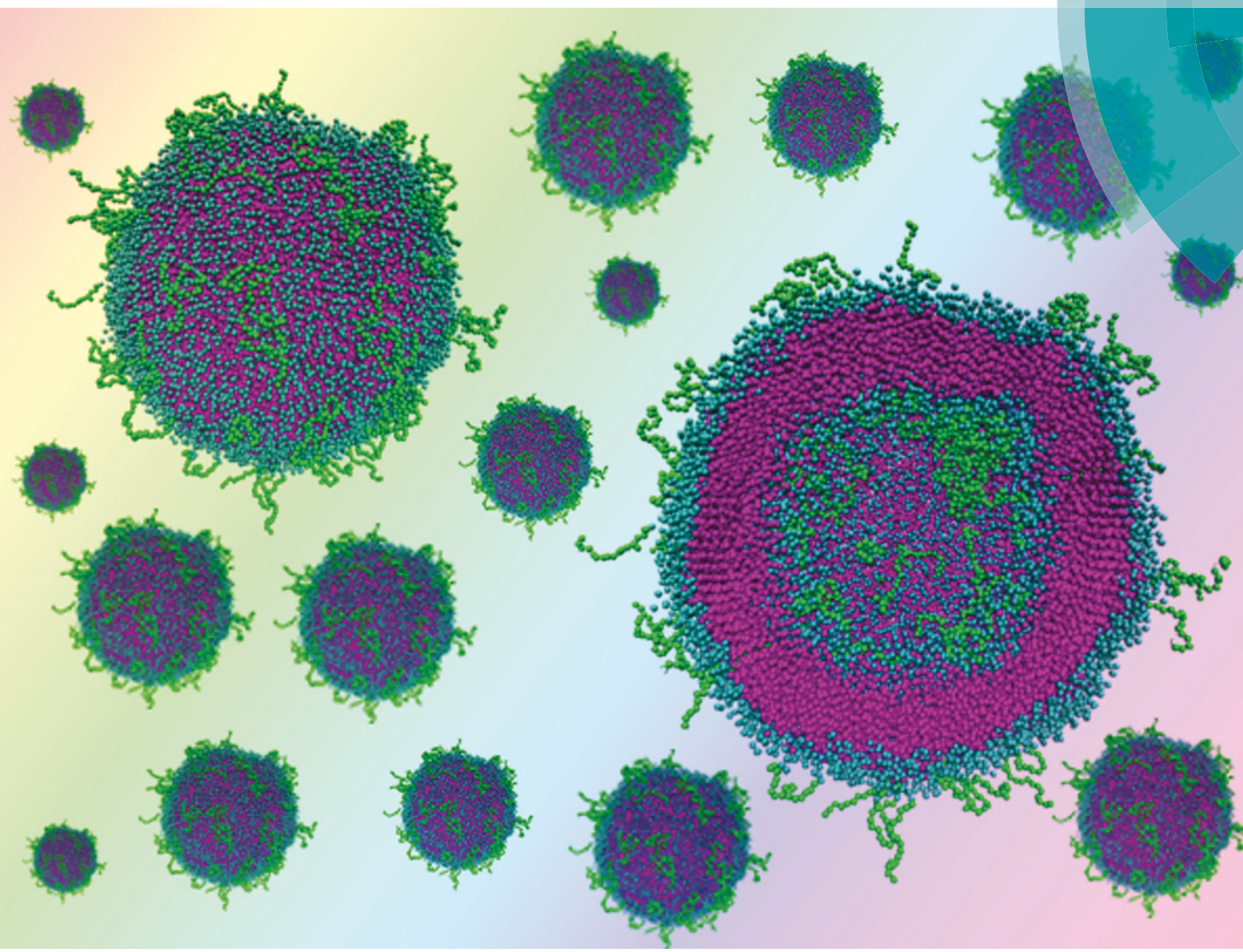

ISSN 2058-9689

ROYAL SOCIETY OF CHEMISTRY

PAPER

Xiang Yu and Meenakshi Dutt

A multiscale approach to study molecular and interfacial characteristics of vesicles

IChemE ADVANCING CHEMICAL ENGINEERING WORLDWIDE

Molecular Systems Design & Engineering

PAPER

View Article Online
View Journal | View Issue

Cite this: *Mol. Syst. Des. Eng.*, 2018, 3, 883

A multiscale approach to study molecular and interfacial characteristics of vesicles†

Xiang Yu and Meenakshi Dutt *

The functions of colloids, such as membranes and vesicles, are dictated by interfacial properties which are determined by an interplay of physical interactions and processes spanning multiple spatiotemporal scales. The multiscale characteristics of membranes and vesicles can be resolved by the hybrid molecular dynamics-lattice Boltzmann technique. This technique enables the resolution of particle dynamics along with long range electrostatic and hydrodynamic interactions. We have examined the feasibility of an implementation of the hybrid technique in conjunction with a Martini-based implicit solvent coarse-grained force field to capture the molecular and interfacial characteristics of membranes and vesicles. For simplicity, we have examined two types of vesicles whose molecular components have different sustained interactions with the solvent. One of the vesicles encompassed phospholipids and the other vesicle was composed of phospholipids and poly ethylene glycol (PEG)-grafted lipids. The molecular and interfacial characteristics of the phospholipid vesicle and PEGylated, or hairy, vesicles are found to be in good agreement with earlier experimental, computational and theoretical findings. These results demonstrate that the multiscale hybrid technique used with a Martini-based implicit solvent coarse-grained model is suitable for capturing the molecular and interfacial characteristics of membranes and vesicles. Furthermore, other implicit solvent coarse-grained models can be used in conjunction with the hybrid molecular dynamics-lattice Boltzmann technique to examine the molecular and interfacial characteristics of membranes and vesicles. Our study demonstrates the potential of the hybrid technique in capturing multiscale interfacial characteristics of intra- and inter-colloid interactions in suspensions under different flow conditions, and their relation to molecular properties. In addition, this technique can be applied to design colloids with multiscale characteristics which yield desired interactions with other colloids and responses to external stimuli.

Received 30th May 2018,
Accepted 26th September 2018

DOI: 10.1039/c8me00029h

rsc.li/molecular-engineering

Design, System, Application

Colloidal suspensions are critical for a wide range of technological applications due to their complex interfacial properties. The surface chemistry and profile of colloids dictate their stability, response to external stimuli and self-organization in suspensions. The complexity of the interfacial characteristics of colloids arises from the combination of physical interactions and processes spanning large spatiotemporal scales which impact the structural and dynamical properties of these systems. Hence, the multiscale characteristics of colloidal particles are impacted by the molecular scale, long range electrostatic, hydrodynamic interactions and their interplay. A fundamental understanding of the links between the molecular composition (such as solvophilic segment length, or relative concentration), the interfacial and collective properties of colloids requires consideration of their multiscale characteristics. This understanding can be harnessed to design colloidal particles with desired characteristics. The proposed approach can be applied to probe multiscale characteristics of the interactions between colloids in suspensions under different flow conditions, and their relation to molecular properties. Furthermore, the hybrid molecular dynamics-lattice Boltzmann technique in conjunction with a Martini-based implicit solvent coarse-grained model can be adopted to design colloidal particles with specific molecular compositions which yield desired interactions with other colloidal particles and responses to external stimuli.

Introduction

Colloids are critical for a wide range of technological applications due to their complex interfacial properties. The surface chemistry and profile of colloids dictate their stability, response to external stimuli and self-organization in suspensions. The complexity of the interfacial characteristics of colloids arises from the combination of physical interactions and processes spanning large spatiotemporal scales which impact their structural and dynamical properties. Hence, the multiscale characteristics of colloids are impacted by the molecular scale, long range electrostatic, hydrodynamic interactions and their interplay. A fundamental understanding of

Chemical and Biochemical Engineering, Rutgers, The State University of New Jersey, Piscataway, NJ 08854, USA. E-mail: meenakshi.dutt@rutgers.edu

† Electronic supplementary information (ESI) available. See DOI: 10.1039/c8me00029h

the links between the molecular composition, the interfacial and collective properties of colloids requires consideration of their multiscale characteristics. This fundamental understanding can be harnessed to design colloids with desired interactions with other colloids, responses to external stimuli and characteristics under flow. Whereas experimental approaches can provide insight into the multiscale characteristics of colloids, limitations in their spatiotemporal resolution gives rise to the need for suitable computational approaches.

A single computational approach which addresses physical interactions at disparate spatiotemporal scales is well suited to identify the predominant factors and mechanisms responsible for the characteristics of colloids. Of specific interest is the ability to determine molecular and interfacial characteristics of

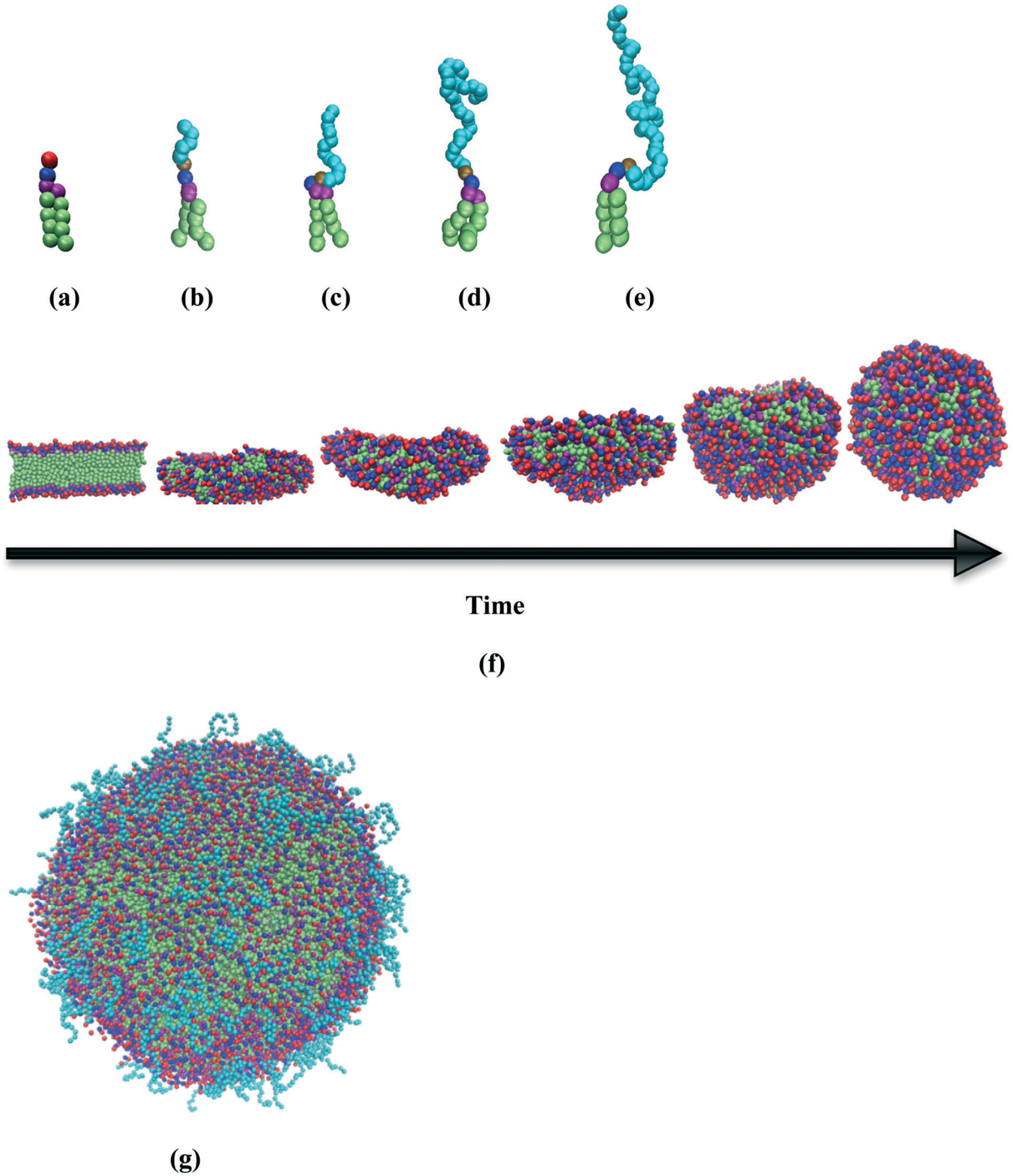

Fig. 1 Coarse grained model of (a) DPPC, PEG-DPPE with PEG chain length of (b) 6, (c) 12, (d) 28, and (e) 45. The red, blue, and purple beads represent the head group bead types Q0, Qa and Na, respectively. The green beads represent the hydrophobic tail beads (type C1). The cyan and brown beads represent bead types SP2 and N0, respectively. (f) Closing of a DPPC planar-membrane encompassing 814 DPPC molecules to form a stable vesicle. (g) Hairy vesicle with PEG 12 chains grafted to DPPC molecules which are present at a concentration of 10%.

colloids using such an approach. In this study, we use a computational approach which captures the particle dynamics and the hydrodynamic interactions in colloids. We focus on two types of colloids whose molecular components have different levels of sustained interactions with the solvent. One class of the colloids (namely, a planar-membrane and a vesicle) encompasses amphiphiles with small hydrophilic groups (compared to the hydrophobic groups), as shown in Fig. 1. The other class of colloids (namely, vesicles) encompasses two types of amphiphilic molecules with one of the molecules bearing a long hydrophilic group which extends into the aqueous medium, as shown in Fig. 1.

Potential particle dynamics-based approaches such as multi-particle collision dynamics[1–5] and dissipative particle dynamics[4,6–10] are suitable for simultaneously resolving particle dynamics while capturing the hydrodynamics of colloidal systems.[11–13] However, these approaches are typically restricted to values of the Schmidt number (*i.e.*, the ratio of the diffusive momentum transfer rate to the diffusive mass transfer rate) which are considerably lower than that corresponding to water at standard temperature and pressure,[14,15] although efforts have been made to address this gap.[16] In addition, the soft repulsive interactions in dissipative particle dynamics are unable to accurately capture the structure of molecules within colloids.[17] Another approach[18] integrates hydrodynamic forces into intra and inter-molecular interactions. Yet it is not clear if this approach yields the long-tail behavior characteristic of hydrodynamic interactions.

We use a hybrid approach interfacing a continuum fluid dynamics technique known as the lattice Boltzmann method (LBM)[19,20] to the classical molecular dynamics (MD) method. This approach has been developed to simultaneously capture deterministic particle dynamics, hydrodynamic interactions and thermal fluctuations,[14,15] and is used to examine colloidal suspensions and flow.[6,7] The hybrid approach is suitable for addressing collective phenomena in colloidal systems where individual colloids continuously maintain an interface with the solvent. The dynamics of the particles constituting the colloids is resolved by the MD simulation technique.[21–24] The fluid and its dynamical properties is modeled by the LBM[19,20] which yields a hydrodynamic description provided by the Navier–Stokes equation that is valid down to very short spatiotemporal scales. Hence, the solution to the Navier–Stokes equation for the flow field around a particle is accurate for distances greater than a few lattice spacings.[14,15] Similarly, an all-atom MD representation will hypothetically yield hydrodynamic behavior for distances greater than a few water molecule diameters.[25] The two approaches (namely, MD technique and LBM) are equivalent as long as they produce the same long-range flow field.[14,15] The two techniques are coupled to enable the colloids and fluid to exchange momentum and introduce hydrodynamic interactions between the colloids. Hence, this approach enables the resolution of the impact of both long range hydrodynamic and electrostatic forces on the colloidal dynamics.

There exist multiple implementations of the hybrid molecular dynamics-lattice Boltzmann method (MDLBM).[14,15,25–28] An earlier implementation[29] models a colloid by point particles on its surface which interacts with the fluid through a set of bounce-back rules. Thermal fluctuations are introduced into this implementation to study Brownian motion.[30] An alternate implementation[14,15] uses a frictional force proportional to the difference in the local velocities of the colloid and fluid, and modeled large colloids by representing their surface *via* a collection of smaller MD particles. Thermal fluctuations are introduced *via* a Langevin thermostat acting on the MD particles and fluctuating LB fluid.[26] This approach has been extended to examine the dynamics of polyelectrolytes and charged colloids with long range electrostatic interactions.[15] Another implementation[25,27,28] uses a force coupling method which removes the need for an external Langevin thermostat acting on the colloids, and accounts for thermal fluctuations. Existing methods are also used to study the dynamics of single, large colloids[14,15,25,27,30] or macromolecules[15,31,32] in solution. However, these methods have not been extended to study the multiscale structural and dynamical characteristics of colloidal suspensions or emulsions.

We demonstrate the feasibility of a MDLBM implementation which includes aspects of the earlier methods to capture the multiscale structural and dynamical characteristics of colloids. We study the impact of hydrodynamics on the molecular characteristics of pure phospholipid planar-membranes and vesicles, and two component hairy vesicles encompassing DPPC (dipalmitoylphosphatidylcholine) and poly ethylene glycol (PEG)-grafted DPPC (or, hairy lipids). These two vesicles are selected to be simplified representations of colloids. The amphiphilic molecules in the vesicles have different degrees of sustained interactions with the solvent. The head groups of the phospholipid molecules and the PEG chains grafted to the lipid head groups maintain their interactions with the fluid through the duration of the study. The PEG chains adopt extended conformations in the solvent as compared to the lipid head groups. The different degrees of sustained interactions of the molecules with the solvent can potentially impact their organization and dynamics in the vesicle bilayer along with their conformation in the solvent. The pair and non-pair interactions between the MD particles is represented by a coarse grained implicit solvent model which is based upon the dry Martini force field.[33]

As a part of the study, we investigate the molecular properties of phospholipids and PEGylated lipids in liposomes and hairy vesicles, respectively. Our results for the molecular characteristics of DPPC in a vesicle bilayer are good agreement with corresponding results from experiments and other simulation studies. In addition, the characterization results for the PEG chains on the surface of the hairy vesicles and their trends, as a function of relative concentration and length of the PEG chains, are in agreement with existing theoretical and experimental studies. Our results validate the use of the hybrid MDLBM technique in conjunction with a coarse-grained implicit solvent force field for modeling colloids.

Our study can be potentially extended to apply this technique to probe multiscale characteristics of the interactions

between colloids in suspensions under different flow conditions, and their relation to molecular properties. Furthermore, the hybrid MDLBM technique in conjunction with a Martini-based implicit solvent coarse-grained model can be adopted to design colloids with specific molecular compositions which yield desired interactions with other colloids, responses to external stimuli and characteristics under flow.

Methods

Hybrid molecular dynamics-lattice Boltzmann method

The dynamics of the particles constituting the colloids is resolved *via* the MD simulation technique using the canonical ensemble with a Langevin thermostat. The dynamics of the fluid is resolved through LBM with thermal fluctuations, based upon an earlier implementation.[25,27,28] The hydrodynamic interactions impact the particle dynamics by coupling LBM with the MD technique. At each time step, the momenta of the fluid and the MD particles are coupled through their microscopic relations at the fluid–solid boundary but resolved and independently updated by the respective methods.

In an earlier implementation of LBM,[27] a large spherical colloid is modeled through its surface which encompasses a network of evenly distributed node particles. The node particles enable interactions between the fluid and the colloid. These interactions are distributed to the lattice sites in the vicinity of the node particles. Mesh effects are prevented by setting the number of node particles to sufficiently large values such that the distance between each of the node particles is smaller than the lattice spacing Δx. The mass of the colloids is the sum of the mass of the individual node particles. However, discretizing the surface of an individual coarse-grained MD bead (which is part of a coarse-grained representation of an amphiphile) into a network of node particles is computationally expensive. Given the large number of hydrophilic lipid MD beads which will interface with the fluid, the computational cost of calculating all the intermolecular interactions between the node particles on the surfaces of two neighboring coarse-grained MD beads will be extremely high. In addition, coarse grained lipid MD beads are essentially point particles with no surface area, which makes it unnecessary to discretize them. These factors remove the need to discretize the surface of each coarse-grained MD bead.

In this study, the lattice Boltzmann fluid is coupled directly to the center of mass of each hydrophilic MD bead by interpolating the mass and velocity of individual coarse-grained MD beads to the nearby fluid lattice sites. The treatment of hydrophilic coarse-grained MD beads as point particles is based upon another implementation of LBM,[14] where the mass of the particle is distributed using linear interpolation. In this study, the immersed boundary method[34] is applied to interpolate the point particles to the local fluid lattice sites. This approach has been demonstrated by several investigations to be more effective in distributing singular force densities, thereby reducing mesh effects for point particle-like objects.[28,35] Similar to this implementation, the coupling between the LB fluid and the MD particle is modeled through a friction force that is proportional to the velocity difference between the center of mass of the MD particle and LB fluid:

$$F_{xy} = \gamma(V_y - U_f)\xi_{xy}$$

$$F_y = -\gamma(V_y - U_f)$$

where F_{xy} represents the local friction force applied on the MD bead y by a lattice site x, γ is coupling parameter, V_y is the velocity of the MD bead y, U_f is velocity of LB fluid interpolated to the MD particle position based upon local lattice sites, and ξ_{xy} is interpolation factor so that $\sum_x \xi_{xy} = 1$. According to Newton's third law, the total friction exerted by the MD bead y is reflected back and given by F_y. The coupling parameter γ is modeled by the elastic collision process between the MD point particle and the LB fluid mass:

$$\gamma = \frac{2m_f m_n}{m_f + m_n}\left(\frac{1}{\Delta t_{collision}}\right)$$

where m_n is the mass of a lipid head MD bead in contact with fluid, and m_f is the mass of the fluid colliding with each hydrophilic MD bead. Since we treat MD particles as point particles, the fluid mass at each interpolation position is calculated as $\rho\Delta x^3$, where ρ is bulk fluid density (set as the density of water at the corresponding temperature) and Δx is lattice space (set as 10 nm). In this study, the mass of all MD beads are set to 72 g mol^{-1} with exception to the PEG bead whose mass is set to 45 g mol^{-1}. The collision time $\Delta t_{collision}$[27] is related to the bulk fluid property (that is, the density and viscosity η)

$$\eta = \frac{1}{3}\rho\left(\Delta t_{collision} - \frac{dt}{2}\right)\left(\frac{dx}{dt}\right)^2,$$

where dx is lattice space, dt is MD time step and the speed of sound is set as $\frac{1}{\sqrt{3}}\frac{dx}{dt}$.

Interaction parameters between MD particles

The effective chemistry between the MD particles is captured by the pair and non-pair interactions. The forces and potential energies associated with pair, bond, angle and dihedral interactions requires an implicit solvent model. Existing solvent-free models for lipids have included the chemistry through force matching between all atom and coarse-grained systems;[36–42] Newton inversion method;[36–42] long-range attractive interactions of the hydrocarbon tails,[36–43] hard-

sphere and square well potentials;[36–42] analytical potentials combined with force matching potentials,[36–42] and Lennard-Jones (LJ) potentials for non-bonded interactions between the beads (known as the dry Martini implicit solvent coarse-grained force field).[33] The dry Martini model follows from the standard Martini coarse-grained scheme[43] of grouping approximately four heavy atoms into one bead, and is adopted due to its advantages over the other mentioned models. These advantages include the simplistic form of the interaction potentials and the large range of molecules currently parameterized under the Martini model.[43] In the model, each bead is classified based on its charge, polarity, and ability to form hydrogen bonds. The non-bonded, non-electrostatic pair interactions are modeled by the shifted truncated 12–6 LJ potential with the potential cutoff distance r_c set at 2.5σ for all bead pairs (σ = 0.47 nm). The non-bonded, electrostatic pair interactions are modeled by the shifted Coulombic potential with σ = 0.62 nm. The Coulomb potential $U = \frac{q_1 \times q_2}{4\pi\varepsilon_1\varepsilon_2 r}$, where q_1 and q_2 are the charges on the MD beads, r is the distance between the two charges and ε_1 and ε_2 are the dielectric permittivity, is shifted from r = 0 nm to r = 1.2 nm.[14,33] The bond and angle interactions are modeled respectively by the weak harmonic and cosine harmonic potentials whereas the dihedral is modeled through the CHARMM potential.[33,44,45]

The colloids of interest are vesicles encompassing one or two types of amphiphiles: DPPC and PEG-grafted DPPC molecules, or hairy lipids, as shown in Fig. 1. The interaction parameters for DPPC and PEG-grafted DPPC were obtained from earlier studies.[33,44,45] Non-bonded interactions of the hairy lipids using the standard Martini model were modified to compensate for the loss of the solvent. In an earlier study,[44,45] the PEG–PEG interaction was modeled as a SNda–SNda interaction whereas the PEG–DPPC interaction was treated as N0-x where x represents the different bead types in the DPPC molecule. However, using the dry Martini model, the PEG beads were observed to embed themselves into the hydrophobic region of the vesicle bilayer. In addition, with increase in the PEG concentration, multiple PEG chains were observed to coil together. These observations demonstrated that the PEG–PEG and PEG–DPPC interactions in the dry Martini model were highly enthalpically favorable. Intuitively, the lack of the solvent would remove the effects of hydration and hydrogen bonding on the behavior of the solute beads (that is, PEG and hydrophilic lipid head beads), and therefore increase the favorable enthalpic interactions. This difficulty was overcome by treating the PEG–DPPC interaction as a P2–DPPC interaction and the PEG–PEG interaction as a SP2–SP2 interaction. The bead types P2 and SP2 are from the Martini force field.[43] This change maintains the same interaction energy level between the PEG and DPPC hydrophilic groups (Choline Qa, Phosphate Q0, and glycerol Na), but decreases the interaction between the PEG beads and the hydrophobic beads of DPPC, namely C1.

The implicit solvent model of PEG and the lattice Boltzmann fluid as a good solvent are validated through measurements of the probability of the end to end distance of the PEG chain.[46] A planar-membrane composed of 814 DPPC lipids with a PEG 19 chain (molecular weight ~838 g mol^{-1}) grafted to one of the lipid head groups was simulated for approximately 100 ns. Multiple independent trajectories (namely, 500) were used to calculate the end to end distance. Results from MDLBM with the coarse grained implicit solvent model and MD simulations using the standard Martini model were compared (see Fig. 2). Correspondence in the results from MDLBM with the coarse-grained implicit solvent model and the standard Martini model validates the former.[46] In addition, the radius of gyration of single PEG chains of different lengths were computed and examined as a function of the corresponding molecular weight, as shown in Fig. 3. The scaling exponents relating the radius of gyration to the molecular weight were determined to be 0.5876 and 0.553, and found to be in good agreement with those from an earlier study[44] using the standard Martini model (~0.57 and 0.51 respectively). This result validates the model for the PEG chain.

System setup and simulation details

The open source community-based MD package entitled LAMMPS[48] was used for this study. The two colloids of interest were: a pure DPPC lipid vesicle and a hairy vesicle encompassing DPPC and hairy lipids. The lipid vesicle was created through the spontaneous fusion of the edges of a pre-assembled square planar-membrane consisting of 814 DPPC lipids. The planar-membrane was placed in a simulation box whose lateral area in the x–y plane was larger than the total area of a monolayer of the planar-membrane. The DPPC lipid planar-membrane was equilibrated in a cubic box of dimensions 40 nm using the canonical ensemble for 1500

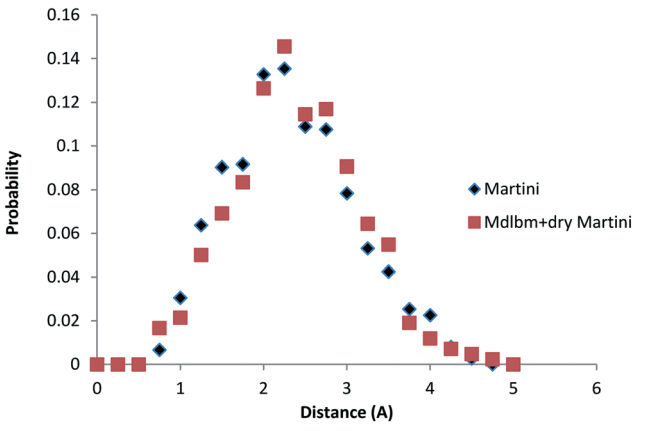

Fig. 2 Probability of the end to end distance of PEG 19 chain. The PEG chain was grafted to a lipid molecule in a planar-membrane composed of 814 DPPC lipids. The planar-membrane was equilibrated at a temperature of 336 K until the area per lipid corresponded with values reported in literature.[47]

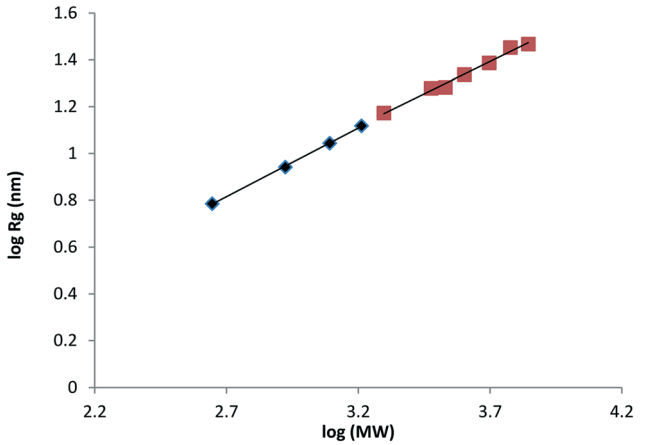

Fig. 3 A plot of the log of the radius of gyration (R_g) (in nm) *versus* log of the molecular weight (MW) for single PEG chains of length 10, 19, 28, 37, 45, 77, 91, 113, 136 and 159. There are two fit lines as the polymer physical behavior differs at lower and higher number of monomers. The measurement was performed using a process similar to that reported by an earlier study.[45]

ns with a time step of 30 fs. Temperature of the system was maintained at 400 K using the Langevin thermostat. Prior studies have demonstrated using the Langevin thermostat on MD beads coupled to the LB fluid lattice reproduces the correct hydrodynamic behavior and particle dynamics.[15,26] Unless stated, the damping rate of the Langevin thermostat was set to 2000 fs, which maintains the desired temperature.[33] This temperature was higher than 314 K, the transition temperature of DPPC,[49] to ensure that the bending energy of the planar-membrane was lower than its interfacial energy. This allowed the planar-membrane to minimize its interfacial energy by bending and fusing its edges to form a vesicle, as shown in Fig. 1. This approach prevents the buildup of large asymmetric stresses across the bilayer leaflets which render the vesicle unstable. This simulation was performed in the absence of the LB fluid. After the vesicle was formed, it was 'immersed' into the LB fluid by coupling the hydrophilic head beads of the lipids to the fluid lattice. The lipid head beads were coupled to the LB fluid as these beads were exposed to the LB fluid for the entire duration of the simulations. The time step was maintained at 10 fs to ensure 1 : 1 ratio of the lattice space to the timestep.

Some of the measurements were required to be performed on a DPPC planar-membrane. For this purpose, a planar-membrane encompassing 3265 DPPC lipids was preassembled. The planar-membrane was equilibrated using the MD technique in the canonical ensemble at a temperature of 310 K and a pressure of 1 bar, for 15 ns at a time step of 30 fs. The Langevin thermostat and the Berendsen barostat were used. The dimension of the simulation box was fixed along the z-direction so that planar-membrane could only expand along the x- and y-directions with the modulus set to 3333 atm (corresponding to a compressibility of 3×10^{-4} atm^{-1}) and the damping rate given by 1000 fs. The equilibrated planar-membrane was immersed in a LB fluid with the lipid hydrophilic head groups coupled to the fluid lattice, and was equilibrated for another 10 ns at a time step of 10 fs. The simulation box volume was kept constant to maintain the lattice spacing fixed. Therefore, the canonical ensemble was used to equilibrate the planar-membrane using MDLBM.

The vesicle and planar-membrane systems simulated using MD and MDLBM were characterized when the bilayer was in the gel and fluid phases. The gel and fluid phases of DPPC correspond respectively to temperatures of 310 K and 336 K.

The hairy vesicle composed of DPPC and hairy lipids was preassembled using 3265 amphiphilic molecules. The relative concentration of the hairy lipids was varied from 2.2% to 20%. In addition, the length of the PEG chains was varied (that is, the number of beads encompassing the PEG chains was set to 6, 12, 28 and 45). Each system was equilibrated using MDLBM in the canonical ensemble at a temperature of 336 K using the Langevin thermostat for 50 ns with a time step of 10 fs. Each system was simulated for an additional 10 ns to perform measurements of the system properties. The lipid head groups and the PEG beads were coupled to the LB fluid during the MDLBM simulations. Three independent particle trajectories were used for the characterization of each vesicle.

Results and discussion

(A) Molecules in vesicles with reduced conformations in the solvent

The organization and collective dynamics of the lipid molecules will be impacted by the interfacial characteristics of the molecules in the vesicle. The dynamics and packing of DPPC molecules in a pure phospholipid vesicle was determined using MDLBM. These molecular properties were characterized through the diffusion coefficient and the area per lipid. The use of the centers of mass of the lipids for measurements of the diffusion coefficient through the mean square displacement yields larger values of the diffusion coefficient as well as nonlinear mean square displacement curves in the first few nanoseconds. This observation has been attributed to the fact that the dynamics of the lipid tails is faster than the lipid head groups.[50] This is known as the tail-wagging effect.[50] To prevent the tail-wagging effect, the mean square displacement of 200 head beads of the DPPC lipid molecules were measured for 90 ns. Measurements from time 15 ns to 75 ns were used to determine the diffusion coefficient. To circumvent the impact of the bilayer curvature, the diffusion coefficient of the phospholipids in the outer and inner leaflets of the vesicle bilayer were measured separately. In addition, the diffusion coefficient of the lipids in a DPPC planar-membrane was measured with the goal of comparing the results with corresponding findings in a vesicle. Since the vesicle and the planar-membrane were free to move during the span of the simulation, the mean square displacements of the center of mass of the vesicles and planar-membranes were subtracted from the measurements of those for the lipids. To improve the statistical accuracy of the

measurement, the mean square displacement of the lipids at time τ was estimated to be the average of the difference between the mean square displacements (MSD) at time step = t_o and step = $t_o + \tau$.

$$\mathrm{MSD}(\tau) = \frac{1}{N_t}\sum_{n=0}^{N_t}\frac{1}{N}\sum_{i=1}^{N}\left|R(n+\tau) - R(n)\right|^2$$

where $R(t)$ is the displacement of a particle at time t, N_t is total number of intervals the mean square displacements are averaged over, and N represents the number of lipids used for the calculation. A similar approach was used in earlier studies.[51,52] Fig. 4(A to D) shows the mean square displacements of the DPPC lipids (for τ ranging from 0 to 2 000 000 iterations) at 310 K and 336 K, both with and without the LB fluid.

Fig. 4 shows the lipids in the outer monolayer to move faster than those in the inner monolayer. This observation is based upon the packing of the molecules; lipids in the outer monolayer tend to pack less tightly than those in the inner monolayer. Earlier studies[53] have demonstrated that whereas the overall tension in the bilayer of the vesicle is zero, the tension in the inner leaflet of a vesicle is negative, while the outer leaflet has a positive tension. The lipid molecules will pack with higher or lower density in monolayers with respectively negative or positive tension. The density of the molecular packing will impact the mobility of the molecules. A molecule in a monolayer that is under negative tension will encounter many more "obstacles" or neighboring molecules (as compared to a monolayer under positive tension) as it diffuses in the monolayer. Hence, molecules in a monolayer that is under negative tension will have a smaller diffusion coefficient than molecules present in a monolayer under positive tension. Our observation agrees with earlier studies.[54–56] Furthermore, a curved bilayer has been known to have a lower lipid packing density than a planar bilayer.[57] Therefore, the dynamics of the lipids in planar-membranes will be slower than those in either leaflet of the vesicle bilayer as demonstrated by our measurements. This result shows the dynamics of the lipids at a given temperature to be related to their molecular chemistry and environment.

To understand the impact of the LB fluid on the dynamics of the lipid molecules, the diffusion coefficient (D) of the lipids was calculated using the slope of the interpolation of the mean square displacements:

$$D = \frac{1}{2d} \times k \times \frac{1}{\text{timestep}}$$

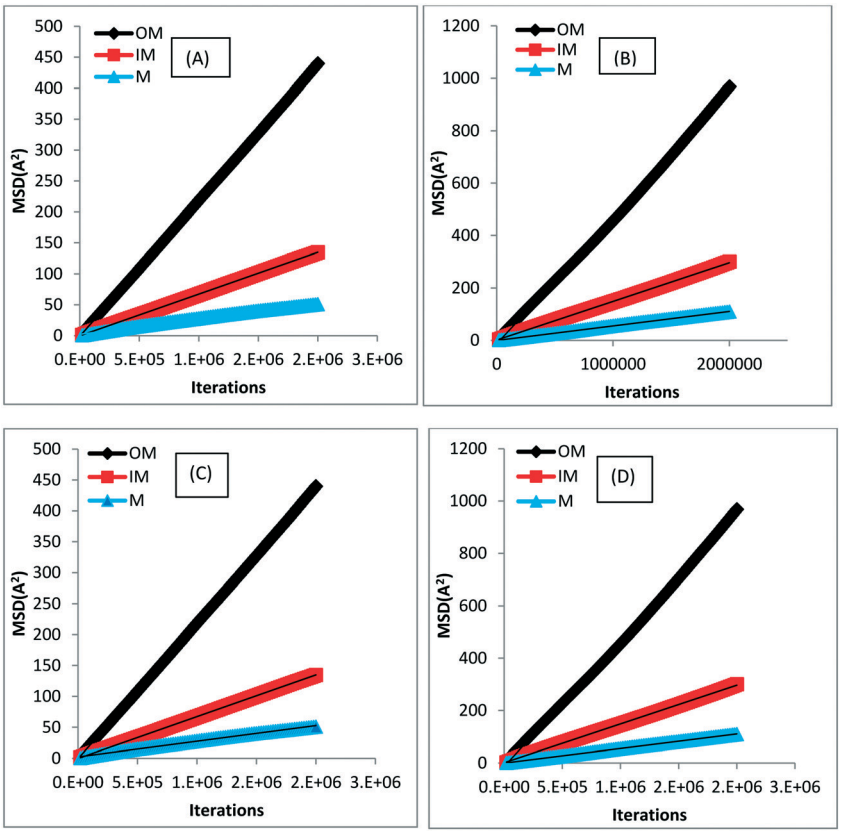

Fig. 4 (A) The mean square displacements (MSD) at 336 K with LB fluid; (B) MSD at 336 K without LB fluid; (C) MSD at 310 K with LB fluid, and (D) MSD at 310 K without LB fluid. Number of lipids used in all three measurements are same (OM: outer monolayer. IM: inner monolayer. M: planar-membrane).

The variable d is 2 and 3 respectively for planar-membranes and vesicles. The small dimension of the vesicles will magnify the impact of curvature on the MSD of the lipid molecules. Hence d is set to 3 for the measurements of the MSD of the lipid molecules in the vesicles. Table 1 summarizes the diffusion coefficient of DPPC lipids in a planar-membrane and vesicle at 310 K and 336 K, with and without the LB fluid.

The measurements summarized in Table 1 demonstrate the lipids to diffuse faster in the presence of the LB fluid. We surmise that a particle immersed in the LB fluid passes its momentum to nearby particles by creating a flow field in the fluid. The force from the flow field produced by the original particle will accelerate the neighboring particles. The differences between the results from experiments (see Table 1) and our simulations arises as the experiments typically use giant unilamellar vesicles for the measurements. These colloids are sufficiently large that the curvature of the vesicles could be ignored. However, the simulations examined a vesicle of average diameter of 15 nm which is significantly smaller than what is typically used in experimental studies. Therefore, the experimental measurements of the diffusion coefficient are akin to studying the dynamics of lipids on a planar-membrane. Hence, our measurements of the diffusion coefficient for the phospholipids in planar-membranes in the fluid and gel phase are in agreement with corresponding experimental (see Table 1) and computational studies.[58,59]

Further insight into the molecular packing of the lipids can be obtained through the measurements of the area per lipid. Table 2 summarizes the area per lipid of planar-membranes and vesicles, in the absence and presence of the LB fluid, at temperatures of 310 K and 336 K. The measurements show the area of per lipid of a planar-membrane is smaller than the area per lipid for vesicles in fluid and gel phase. Also, the area per lipid in the outer-monolayer is much larger than a corresponding measurement in the inner monolayer of the vesicle. This observation is independent of the temperature and the presence of the LB fluid. Furthermore, the measurements show that coupling the hydrophilic lipid head groups to the LB fluid does not impact the packing of the molecules in both monolayers. Our measurements indicate that the lipids are more tightly packed in the inner monolayer of the vesicle than the outer monolayer. The tightness of the packing of the lipid molecules is responsible for the difference in the values of the area per lipid corresponding to a planar-membrane, and the inner and outer monolayers of a vesicle. This tightness of the lipid packing is also reflected in the measurements of the diffusion coefficient for lipid molecules in a planar-membrane and a vesicle. The measurements for the planar-membrane and vesicle in the gel phase are observed to be in good agreement with experimental values (see Table 2).[47,60,61] Our results also match those from previous studies which have shown that area per lipid and diffusion coefficient of the lipids are intercorrelated.[62–65]

Table 2 Area per lipid of DPPC molecules in vesicles and planar-membranes, in the absence and presence of the LB fluid, at temperatures of 310 K and 336 K (OM – outer monolayer. IM: inner monolayer)

Temperature		336 K	310 K
Planar-membrane	No LB fluid (Å^2)	64.3 ± 0.2	62.9 ± 0.2
	LB fluid (Å^2)	64.4 ± 0.2	62.5 ± 0.2
Vesicle	No LB fluid (Å^2)	OM: 94.6 ± 0.5	OM: 92.1 ± 0.5
		IM: 68.0 ± 2	IM: 64.0 ± 1.0
	LB fluid (Å^2)	OM: 94.2 ± 0.4	OM: 91.8 ± 0.5
		IM: 67.0 ± 2	IM 64.0 ± 1.0
Experimental (Å^2)[47,60,61]		~67	~63

4.2. (B) Molecules in vesicles with extended conformations in the solvent

The interfacial properties of a colloid encompassing amphiphilic molecules bearing solvophilic chains can be determined by characterizing the properties of these molecules. Hairy vesicles were used to investigate the characteristics of the amphiphilic molecules in the vesicles with extended conformations in the solvent. The hairy vesicle encompassed a binary mixture of phospholipid DPPC and PEGylated phospholipids PEG-DPPE, which were present in different relative concentrations. In addition, PEG chains of different molecular weights or lengths were also studied (namely, 6, 12, 28 and 45). We examined the impact of the length and relative concentration of the PEG chains on their conformational characteristics. We performed the measurements of these characteristics using MDLBM. Our investigations provide insight on the conformational characteristics of the PEG chains and their comparison with existing theory.

The conformations of the PEG chains can be characterized *via* the radius of gyration. The radius of gyration is measured for each PEG chain in a given bilayer leaflet and averaged over all the chains in the leaflet. Fig. 5 shows the measurements of the radius of gyration for different PEG chain lengths and relative concentrations in the outer leaflet of the hairy vesicle bilayer. The radius of gyration (R_g) and molecular

Table 1 Diffusion coefficient of DPPC lipids in planar-membrane and vesicles, in the absence and presence of the LB fluid. The measurements were performed at temperature corresponding to the gel (310 K) and fluid phase (336 K) of a DPPC bilayer

		Outerlayer (m^2 s^{-1})	Innerlayer (m^2 s^{-1})	Planar-membrane (m^2 s^{-1})	Literature[58,59]
310 K	No fluid	2.6722×10^{-11}	8.20444×10^{-12}	4.625×10^{-12}	$\sim 2.10 \times 10^{-12}$
	LB fluid	3.656×10^{-11}	1.12517×10^{-11}	6.303×10^{-12}	
336 K	No fluid	2.8707×10^{-11}	1.05917×10^{-11}	2.220×10^{-12}	$\sim 2.25 \times 10^{-11}$
	LB fluid	6.0796×10^{-11}	2.06467×10^{-11}	1.089×10^{-12}	

weight (MW) are related through the following scaling relation $R_g \sim MW^a$. The scaling exponent a is determined to lie in the range of 0.61 to 0.63 (see ESI† Fig. SI1 for scaling exponent measurements). The value for exponent a agrees with the corresponding value for a free PEG chain in a LB fluid, as shown in Fig. 3. This result implies that the scaling relation between the radius of gyration and the molecular weight of a PEG chain is independent of its grafting density, length and curvature of the grafting surface.

As expected, the radius of gyration is observed to increase with the length of the PEG chain. In addition, the increase in the radius of gyration becomes more pronounced with the relative concentration of the PEG chains. For low grafting densities or relative concentrations, the PEG chains do not interact with each other laterally and adopt 'mushroom-like' conformations. For high grafting densities, the PEG chains avoid interacting with each other laterally by adopting increasingly 'stretched-out', or 'brush-like' conformations.[45,66,67] To determine whether the PEG chains transition from a mushroom to a brush regime, we determine the end-to-end distances for each system in the presence of the LB fluid (as shown in Fig. 6). The end-to-end distance is given by the distance between the center of mass of the last bead of the PEG chain and its grafting point on the lipid molecule.

The end-to-end distance is observed to increase with the PEG chain length and relative concentration. We observe a rapid increase in the end-to-end distance for PEG 28 and 45 at around 10% concentration of the PEG chains. This behavior is indicative of a change in the conformation of the PEG chains. To determine whether the PEG chains transition from a mushroom to a brush conformation, the scaling of the end-to-end distance with the degree of polymerization (N) and the distance between the grafting points of neighboring PEG chains (D) is measured. D is an average of the distances between each grafting point and its nearest neighbor on the outer monolayer of the vesicle bilayer. Earlier studies[66,67] have shown the PEG chain extension length from a grafting point on a surface to be given by the Flory radius $R_f = aN^{3/5}$ for a chain which adopts a mushroom conformation. The monomer length is given by a which is 0.35 nm. We have found that at low concentration (<5%) of PEG chains, the scaling relation for the PEG chains was in good agreement with the relation corresponding to the mushroom conformation. This result indicates that majority of the PEG chains are adopting a mushroom conformation. As the relative concentration of the PEG chains increase, the end-to-end distance of the PEG chains deviates from that corresponding to the mushroom conformation. The relation between the neighboring grafting point distance D and R_f predict the conformation of the PEG chains.[66–68] When $D < R_f$, the grafted PEG chains are in the brush regime. As shown in Table 3, the shortest PEG chain (that is, PEG 6) is still in the mushroom regime when its concentration reaches 20%. However, for PEG 12, the mushroom to brush transition occurs between the relative concentrations of 10% and 20%. For PEG 28 and 45, the mushroom to brush transition occurs between the relative concentrations of 2.5% and 10%. Hence, our results show the mushroom to brush transition to occur at lower relative

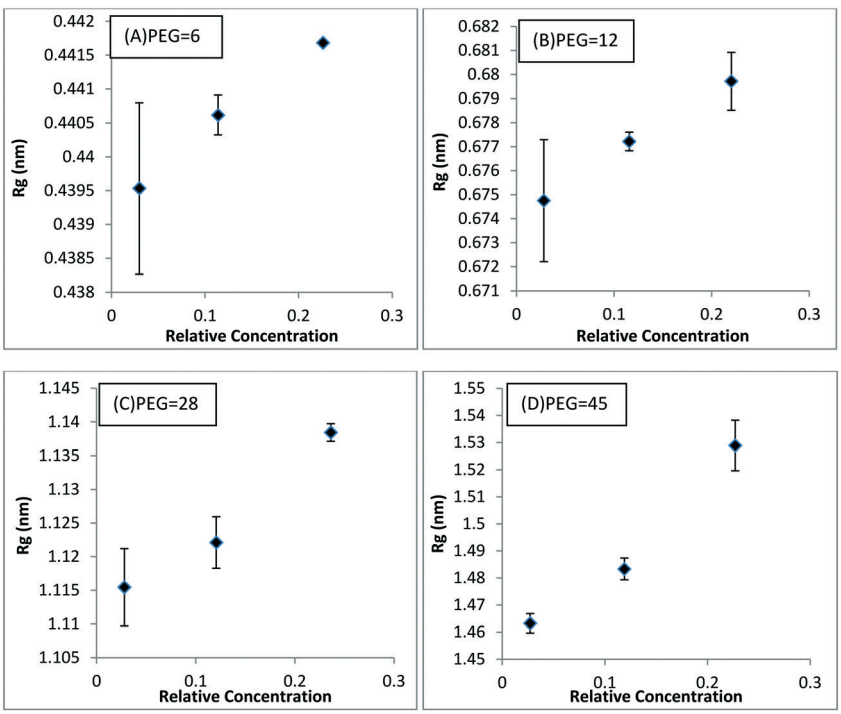

Fig. 5 Radius of gyration (R_g) (in nm) of PEG chain as a function of the relative concentration and length (A = PEG 6, B = PEG 12, C = PEG 28 and D = PEG 45). The relative concentration is defined as the fraction of PEGylated lipids divided by the total number of amphiphiles in the outer monolayer of vesicle.

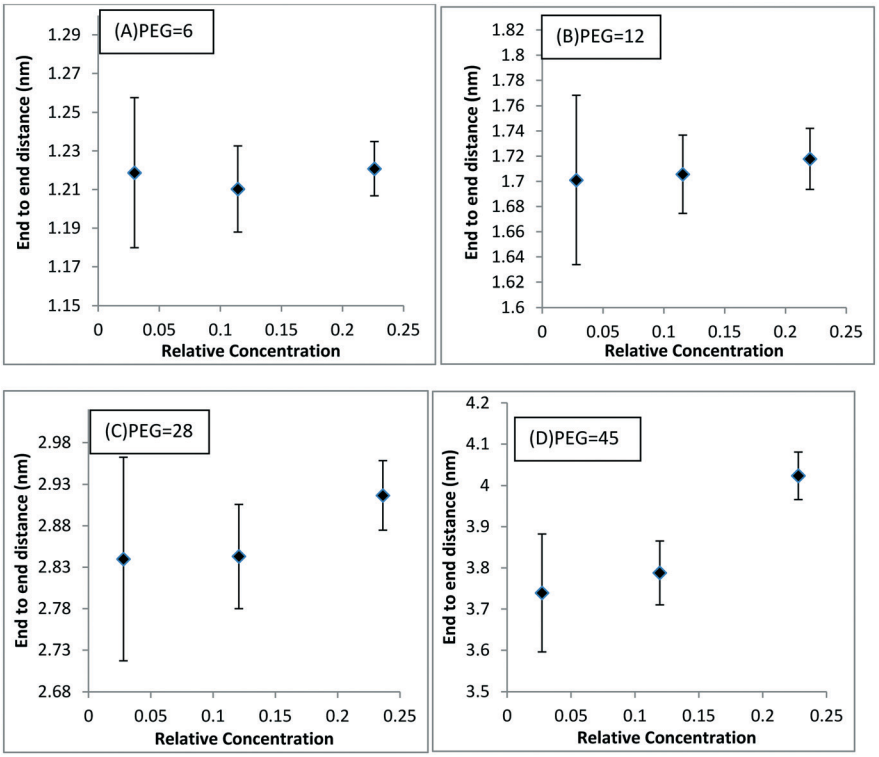

Fig. 6 End to end distance of PEG chain as a function of the outer monolayer PEG chain relative concentration and length (A = PEG 6, B = PEG 12, C = PEG 28 and D = PEG 45). The relative concentration is defined as the fraction of PEGylated lipids divided by the total number of amphiphiles in the outer monolayer of vesicle.

concentrations with increasing PEG chain lengths, which is in agreement with earlier studies.[66]

An earlier study[69] using a similar force field in conjunction with MD simulations qualitatively captured the mushroom to brush transition with increasing concentration of PEG 5000 chains, each grafted to amphiphiles in a bilayer. This finding was validated by experimental investigations[69] and supports our results. However, this study did not couple the solvophilic beads of the amphiphiles to the LB fluid. Another study[70] employed a similar computational approach (but without the coupling to the LB fluid) to study the chain conformations of PEG 5000 grafted to amphiphilic molecules which were present in different concentrations in a lipid bilayer. The measurements of the chain conformations[70] were unable to capture differences in the values for the end-to-end distance and radius of gyration of the PEG chains for different concentrations of the PEG chains. These results demonstrate that hydrodynamic interactions are essential for capturing the conformations of the PEG chains.

Table 3 Distance between neighboring grafting points for different PEG chain lengths and relative concentrations

PEG chain length	6	12	28	45
R_f (nm)	1.026	1.554	2.584	3.436
Relative concentration	D (nm)			
0.022	3.85	3.66	4.04	4.32
0.1	2.01	1.94	2.05	2.04
0.2	1.41	1.51	1.53	1.47

Conclusions

We have implemented a hybrid multiscale computational technique in conjunction with a Martini-based implicit solvent coarse-grained force field and examined its feasibility to capture molecular and interfacial characteristics of membranes and vesicles. For simplicity, we focused on two vesicles: one encompassing DPPC and the other composed of DPPC and PEG-DPPE. The emphasis of this study was the determination of the molecular characteristics of these vesicles using this combined approach. Specifically, we focused on the characteristics of DPPC in the bilayer and the extended conformations of the PEG chains grafted to the vesicle in the solvent.

We measured the diffusion coefficient and area per lipid of DPPC at two temperatures corresponding to the gel and fluid phases of a DPPC bilayer. Our results were in good agreement with corresponding experimental and computational approaches. In addition, our determination of the PEG chain conformational characteristics and trends with PEG chain length and relative concentration agreed with earlier theoretical and experimental studies. We find MDLBM in conjunction with a Martini-based implicit solvent coarse-grained force field to be suitable for capturing molecular and interfacial characteristics of colloidal particles. In addition, the versatility of the approach allows the use of other implicit solvent coarse-grained force fields to be used in conjunction with the hybrid MDLBM technique.

In the future, the application of the hybrid technique in conjunction with a Martini-based implicit solvent coarse-grained force field can be extended to examine the interactions between colloids in a suspension, or the effect of flow on interfaces of colloids, and their relation to molecular characteristics. Hence, this combined approach has the potential to resolve multiscale interfacial, structural and dynamical characteristics of colloids. Furthermore, the approach can be applied to design colloids with suitable molecular compositions which attribute the colloids with desired interactions with other colloids, responses to external stimuli and characteristics under diverse flow conditions.

Conflicts of interest

There are no conflicts to declare.

Acknowledgements

The authors would like to thank Dr. Fikret Aydin and Dr. Leebyn Chong for insightful discussions related to the study. The authors acknowledge that portions of the research were conducted using high performance computing resources provided by XSEDE through award DMR-140125 and Rutgers Discovery Informatics Institute. The authors would also like to acknowledge financial support from the National Science Foundation through award CBET-1644052.

References

1 R. Kapral, Multiparticle collision dynamics: simulation of complex systems on mesoscales, *Adv. Chem. Phys.*, 2008, **140**, 89.
2 E. Allahyarov and G. Gompper, Mesoscopic solvent simulations: Multiparticle-collision dynamics of three-dimensional flows, *Phys. Rev. E: Stat., Nonlinear, Soft Matter Phys.*, 2002, **66**(3), 036702.
3 G. Gompper, T. Ihle, D. M. Kroll and R. G. Winkler, Multi-particle collision dynamics: a particle-based mesoscale simulation approach to the hydrodynamics of complex fluids, in *Advanced computer simulation approaches for soft matter sciences III*, Springer, Berlin, Heidelberg, 2009, pp. 1–87.
4 G. Gompper, T. Ihle, D. M. Kroll and R. G. Winkler, Advanced computer simulation approaches for soft matter sciences III, *Adv. Polym. Sci.*, 2009, **221**, 1.
5 E. Westphal, S. P. Singh, C. C. Huang, G. Gompper and R. G. Winkler, Multiparticle collision dynamics: GPU accelerated particle-based mesoscale hydrodynamic simulations, *Comput. Phys. Commun.*, 2014, **185**(2), 495–503.
6 R. D. Groot and P. B. Warren, Dissipative particle dynamics: Bridging the gap between atomistic and mesoscopic simulation, *J. Chem. Phys.*, 1997, **107**(11), 4423–4435.
7 M. Dutt, O. Kuksenok, M. J. Nayhouse, S. R. Little and A. C. Balazs, Modeling the self-assembly of lipids and nanotubes in solution: forming vesicles and bicelles with transmembrane nanotube channels, *ACS Nano*, 2011, **5**(6), 4769–4782.
8 M. B. Liu, G. R. Liu, L. W. Zhou and J. Z. Chang, Dissipative particle dynamics (DPD): an overview and recent developments, *Arch. Comput. Methods Eng.*, 2015, **22**(4), 529–556.
9 A. Yazdani, M. Deng, B. Caswell and G. E. Karniadakis, Flow in complex domains simulated by Dissipative Particle Dynamics driven by geometry-specific body-forces, *J. Comput. Phys.*, 2016, **305**, 906–920.
10 I. V. Pivkin, B. Caswell and G. E. Karniadakis, Dissipative particle dynamics, in *Reviews in Computational Chemistry*, ed. K. B. Lipkowitz, 2010, vol. 27, pp. 85–110.
11 H. Noguchi and G. Gompper, Dynamics of vesicle self-assembly and dissolution, *J. Chem. Phys.*, 2006, **125**(16), 164908.
12 A. Grafmüller, J. Shillcock and R. Lipowsky, The fusion of membranes and vesicles: pathway and energy barriers from dissipative particle dynamics, *Biophys. J.*, 2009, **96**(7), 2658–2675.
13 A. Zgorski and E. Lyman, Toward Hydrodynamics with Solvent Free Lipid Models: STRD Martini, *Biophys. J.*, 2016, **111**(12), 2689–2697.
14 P. Ahlrichs and B. Dünweg, Simulation of a single polymer chain in solution by combining lattice Boltzmann and molecular dynamics, *J. Chem. Phys.*, 1999, **111**(17), 8225–8239.
15 V. Lobaskin and B. Dünweg, A new model for simulating colloidal dynamics, *New J. Phys.*, 2004, **6**(1), 54.
16 I. Pagonabarraga, M. H. Hagen and D. Frenkel, Self-consistent dissipative particle dynamics algorithm, *Europhys. Lett.*, 1998, **42**(4), 377.
17 M. Kranenburg, M. Venturoli and B. Smit, Phase behavior and induced interdigitation in bilayers studied with dissipative particle dynamics, *J. Phys. Chem. B*, 2003, **107**(41), 11491–11501.
18 T. Ando and J. Skolnick, On the importance of hydrodynamic interactions in lipid membrane formation, *Biophys. J.*, 2013, **104**(1), 96–105.
19 S. Succi, *The lattice Boltzmann equation: for fluid dynamics and beyond*, Oxford university press, 2001.
20 S. Chen and G. D. Doolen, Lattice Boltzmann method for fluid flows, *Annu. Rev. Fluid Mech.*, 1998, **30**(1), 329–364.
21 F. Aydin and M. Dutt, Bioinspired vesicles encompassing two-tail phospholipids: Self-assembly and phase segregation via implicit solvent coarse-grained molecular dynamics, *J. Phys. Chem. B*, 2014, **118**(29), 8614–8623.
22 V. C. Muthukumar, L. Chong and M. Dutt, Designing soft nanomaterials via the self assembly of functionalized icosahedral viral capsid nanoparticles, *J. Mater. Res.*, 2015, **30**(1), 141–150.
23 A. R. Leach, *Molecular modelling: principles and applications*, Pearson Education, 2001.
24 D. Frenkel and B. Smit, *Understanding molecular simulation: from algorithms to applications*, Elsevier, 2001.
25 S. T. Ollila, C. Denniston, M. Karttunen and T. Ala-Nissila, Fluctuating lattice-Boltzmann model for complex fluids, *J. Chem. Phys.*, 2011, **134**(6), 064902.

26 R. Adhikari, K. Stratford, M. E. Cates and A. J. Wagner, Fluctuating lattice boltzmann, *Europhys. Lett.*, 2005, **71**(3), 473.
27 F. E. Mackay, S. T. Ollila and C. Denniston, Hydrodynamic forces implemented into LAMMPS through a lattice-Boltzmann fluid, *Comput. Phys. Commun.*, 2013, **184**(8), 2021–2031.
28 F. E. Mackay and C. Denniston, Coupling MD particles to a lattice-Boltzmann fluid through the use of conservative forces, *J. Comput. Phys.*, 2013, **237**, 289–298.
29 A. J. Ladd, Numerical simulations of particulate suspensions via a discretized Boltzmann equation, Part 1. Theoretical foundation, *J. Fluid Mech.*, 1994, **271**, 285–309.
30 A. J. Ladd, Numerical simulations of particulate suspensions via a discretized Boltzmann equation. Part 2. Numerical results, *J. Fluid Mech.*, 1994, **271**, 311–339.
31 T. T. Pham, U. D. Schiller, J. R. Prakash and B. Dünweg, Implicit and explicit solvent models for the simulation of a single polymer chain in solution: Lattice Boltzmann versus Brownian dynamics, *J. Chem. Phys.*, 2009, **131**(16), 164114.
32 A. Chatterji and J. Horbach, Electrophoretic properties of highly charged colloids: A hybrid molecular dynamics/lattice Boltzmann simulation study, *J. Chem. Phys.*, 2007, **126**(6), 064907.
33 C. Arnarez, J. J. Uusitalo, M. F. Masman, H. I. Ingólfsson, D. H. de Jong, M. N. Melo, X. Periole, A. H. de Vries and S. J. Marrink, Dry Martini, a coarse-grained force field for lipid membrane simulations with implicit solvent, *J. Chem. Theory Comput.*, 2014, **11**(1), 260–275.
34 A. M. Roma, C. S. Peskin and M. J. Berger, An adaptive version of the immersed boundary method, *J. Comput. Phys.*, 1999, **153**(2), 509–534.
35 R. W. Nash, R. Adhikari and M. E. Cates, Singular forces and pointlike colloids in lattice Boltzmann hydrodynamics, *Phys. Rev. E: Stat., Nonlinear, Soft Matter Phys.*, 2008, **77**(2), 026709.
36 S. Izvekov and G. A. Voth, Solvent-free lipid bilayer model using multiscale coarse-graining, *J. Phys. Chem. B*, 2009, **113**(13), 4443–4455.
37 L. Lu and G. A. Voth, Systematic coarse-graining of a multicomponent lipid bilayer, *J. Phys. Chem. B*, 2009, **113**(5), 1501–1510.
38 A. Lyubartsev, A. Mirzoev, L. Chen and A. Laaksonen, Systematic coarse-graining of molecular models by the Newton inversion method, *Faraday Discuss.*, 2010, **144**, 43–56.
39 Z. J. Wang and M. Deserno, A systematically coarse-grained solvent-free model for quantitative phospholipid bilayer simulations, *J. Phys. Chem. B*, 2010, **114**(34), 11207–11220.
40 A. J. Sodt and T. Head-Gordon, An implicit solvent coarse-grained lipid model with correct stress profile, *J. Chem. Phys.*, 2010, **132**(20), 05B611.
41 E. M. Curtis and C. K. Hall, Molecular dynamics simulations of DPPC bilayers using "LIME", a new coarse-grained model, *J. Phys. Chem. B*, 2013, **117**(17), 5019–5030.
42 A. Srivastava and G. A. Voth, Hybrid approach for highly coarse-grained lipid bilayer models, *J. Chem. Theory Comput.*, 2012, **9**(1), 750–765.
43 S. J. Marrink, H. J. Risselada, S. Yefimov, D. P. Tieleman and A. H. De Vries, The MARTINI force field: coarse grained model for biomolecular simulations, *J. Phys. Chem. B*, 2007, **111**(27), 7812–7824.
44 H. Lee and R. W. Pastor, Coarse-grained model for PEGylated lipids: effect of PEGylation on the size and shape of self-assembled structures, *J. Phys. Chem. B*, 2011, **115**(24), 7830–7837.
45 H. Lee, A. H. de Vries, S. J. Marrink and R. W. Pastor, A coarse-grained model for polyethylene oxide and polyethylene glycol: conformation and hydrodynamics, *J. Phys. Chem. B*, 2009, **113**(40), 13186–13194.
46 S. Redner, Distribution functions in the interior of polymer chains, *J. Phys. A: Math. Gen.*, 1980, **13**(11), 3525.
47 J. F. Nagle and S. Tristram-Nagle, Structure of lipid bilayers, *Biochim. Biophys. Acta, Rev. Biomembr.*, 2000, **1469**(3), 159–195.
48 S. Plimpton, P. Crozier and A. Thompson, *LAMMPS-large-scale atomic/molecular massively parallel simulator*, Sandia National Laboratories, 2007, vol. 18, p. 43.
49 C. H. Huang and S. Li, Calorimetric and molecular mechanics studies of the thermotropic phase behavior of membrane phospholipids, *Biochim. Biophys. Acta, Rev. Biomembr.*, 1999, **1422**(3), 273–307.
50 V. Sundararajan, *Computational modeling of membrane bilayers*, Academic Press, 2011.
51 R. A. Böckmann, A. Hac, T. Heimburg and H. Grubmüller, Effect of sodium chloride on a lipid bilayer, *Biophys. J.*, 2003, **85**(3), 1647–1655.
52 G. Pranami and M. H. Lamm, Estimating error in diffusion coefficients derived from molecular dynamics simulations, *J. Chem. Theory Comput.*, 2015, **11**(10), 4586–4592.
53 M. Antonietti and S. Förster, Vesicles and liposomes: a self-assembly principle beyond lipids, *Adv. Mater.*, 2003, **15**(16), 1323–1333.
54 S. J. Marrink and A. E. Mark, Molecular dynamics simulation of the formation, structure, and dynamics of small phospholipid vesicles, *J. Am. Chem. Soc.*, 2003, **125**(49), 15233–15242.
55 A. R. Braun and J. N. Sachs, Determining structural and mechanical properties from molecular dynamics simulations of lipid vesicles, *J. Chem. Theory Comput.*, 2014, **10**(9), 4160–4168.
56 A. S. Reddy, D. T. Warshaviak and M. Chachisvilis, Effect of membrane tension on the physical properties of DOPC lipid bilayer membrane, *Biochim. Biophys. Acta, Biomembr.*, 2012, **1818**(9), 2271–2281.
57 H. J. Risselada and S. J. Marrink, Curvature effects on lipid packing and dynamics in liposomes revealed by coarse grained molecular dynamics simulations, *Phys. Chem. Chem. Phys.*, 2009, **11**(12), 2056–2067.
58 H. A. Scheidt, D. Huster and K. Gawrisch, Diffusion of cholesterol and its precursors in lipid membranes studied by 1H pulsed field gradient magic angle spinning NMR, *Biophys. J.*, 2005, **89**(4), 2504–2512.
59 G. Lindblom, G. Orädd and A. Filippov, Lipid lateral diffusion in bilayers with phosphatidylcholine,

sphingomyelin and cholesterol: An NMR study of dynamics and lateral phase separation, *Chem. Phys. Lipids*, 2006, **141**(1), 179–184.

60 H. I. Petrache, S. W. Dodd and M. F. Brown, Area per lipid and acyl length distributions in fluid phosphatidylcholines determined by 2H NMR spectroscopy, *Biophys. J.*, 2000, **79**(6), 3172–3192.

61 S. Leekumjorn and A. K. Sum, Molecular studies of the gel to liquid-crystalline phase transition for fully hydrated DPPC and DPPE bilayers, *Biochim. Biophys. Acta, Biomembr.*, 2007, **1768**(2), 354–365.

62 P. G. Saffman and M. Delbrück, Brownian motion in biological membranes, *Proc. Natl. Acad. Sci. U. S. A.*, 1975, **72**(8), 3111–3113.

63 B. D. Hughes, B. A. Pailthorpe, L. R. White and W. H. Sawyer, Extraction of membrane microviscosity from translational and rotational diffusion coefficients, *Biophys. J.*, 1982, **37**(3), 673.

64 B. D. Hughes, B. A. Pailthorpe and L. R. White, The translational and rotational drag on a cylinder moving in a membrane, *J. Fluid Mech.*, 1981, **110**, 349–372.

65 R. Peters and R. J. Cherry, Lateral and rotational diffusion of bacteriorhodopsin in lipid bilayers: experimental test of the Saffman-Delbrück equations, *Proc. Natl. Acad. Sci. U. S. A.*, 1982, **79**(14), 4317–4321.

66 O. Garbuzenko, Y. Barenholz and A. Priev, Effect of grafted PEG on liposome size and on compressibility and packing of lipid bilayer, *Chem. Phys. Lipids*, 2005, **135**(2), 117–129.

67 K. Hristova and D. Needham, The influence of polymer-grafted lipids on the physical properties of lipid bilayers: a theoretical study, *J. Colloid Interface Sci.*, 1994, **168**(2), 302–314.

68 P. de Gennes, Conformations of polymers attached to an interface, *Macromolecules*, 1980, **13**(5), 1069–1075.

69 A. Moretti, B. Zhang, B. Lee, M. Dutt and K. E. Uhrich, Degree of unsaturation and backbone orientation of amphiphilic macromolecules influence local lipid properties in large unilamellar vesicles, *Langmuir*, 2017, **33**(51), 14663–14673.

70 B. Zhang, Modeling impact of amphiphilic macromolecules' degree of unsaturation and hydrophobe conformation on DSPC lipid bilayer, *Doctoral dissertation*, Rutgers University-School of Graduate Studies, 2017.